Engineering of Rare Earth Decorated NiAl Layered Double Hydroxides for Rapid Detoxification of Food Dye from Aqueous Media

Minakshi, Aarti and S. Singhal*

Department of Chemistry, Panjab University, Chandigarh, 160014, India.

*Email:sonal1174@gmail.com ; sonal@pu.ac.in

Received: 2.1.2026, Revised: 26.1.2026, Accepted: 26.1.2026

Abstract

Dye-laden wastewater poses a significant threat to the environment, with fast green dye (FG) emerging as one of the most prevalent contaminants released into aquatic systems. However, the development of novel materials with ultrafast removal performance and consistently high efficiency across a wide pH range remains a major challenge. In this work, a novel and proficient nanoadsorbent was prepared by doping of rare earth element (La) in NiAl-based layered double hydroxide (La/NiAl-LDH). The fabricated nanoabsorbent was validated via different characterization techniques which include P-XRD, FT-IR, TGA, FE-SEM and BET. BET results of La/NiAl-LDH revealed the total surface area of 86.1 m^2/g with pore diameter of 2.9 nm. The fabricated adsorbent was evaluated for elimination of obnoxious pollutant FG with ultrafast adsorption of 94% within 10 min. Additionally, the optimised adsorption conditions in terms of catalyst loading, pH of the solution, contact time and initial pollutant concentration were determined through batch experiments. La/NiAl-LDH exhibited superior performance over a broad pH spectrum. The outstanding regenerability and reusability of La/NiAl-LDH showcase fascinating potential for the cost-effective development of adsorbents with long-term suitability and practicability on large scale.

Keywords

Adsorption; Hydrotalcite; Fast Green, Rare earth element.

1. Introduction

A rapid escalation in water pollution, driven largely by various industrial effluents, has become a growing concern among the scientific communities. Globally, the consumption of contaminated water results in a substantial rise of annual mortality rate from waterborne diseases.[1] The contaminants present in the wastewater may include synthetic food dyes, pharmaceuticals, pesticides and heavy metals.[2] Textile industries discard substantial quantities of synthetic dyes into aquatic systems, which are biologically toxic, highly

persistent and have detrimental effects on the ecosystem.[3] Following China, India ranks as the second largest manufacturer and exporter of dyes, where FG being classified as one of the most encountered and polluting synthetic food dye.[4] Although commonly used as a food colouring reagent, FG is recognized as a potent toxicant that primarily affects the respiratory tract, along with other systemic health risks. Consequently, the development of sensitive and efficient techniques to eliminate FG from wastewater represents a critical and an immediate environmental imperative.

A wide range of physicochemical techniques has been explored for the elimination of synthetic dyes from aqueous media, such as advanced oxidation processes, reverse osmosis, ion exchange methods and adsorption.[5-7] However, each method is constrained by significant practical or economic limitations, whereas, adsorption stands out as the most adaptable, efficient, cost effective and relatively environment friendly technique for wastewater remediation.[8] The efficacy of the adsorption process is predominantly governed by the total surface area, number of pores and surface functionalization of the adsorbent material. Recently, a variety of highly porous adsorbents including metal organic framework (MOFs), biochar, carbon nanotube, MXenes, layered double hydroxides (LDHs) have been documented for elimination of toxicants from wastewater.[9-13]

Among many conventional adsorbents, LDHs have attracted considerable attention owing to their exceptional porosity, tunability, selectivity, high anion exchange capability, facile structural reversibility and substantial adsorptive capacity.[14] LDHs, are two-dimensional (2D) anionic clay compounds with abundant hydroxyl groups, demonstrated by the general formula $[M^{2+}_{1-x}M^{3+}_{x}(OH)_2]^{x+}\ [A^{n-}]_{x/y}.mH_2O$, where M^{2+} and M^{3+} are divalent and trivalent metal cations, respectively. A^{n-} represent intercalated anions of valency n, whereas x is the mole fraction of trivalent metal cations $\frac{M^{3+}}{(M^{3+}+M^{2+})}$ and m stands for number of water molecules.[15] Numerous studies have documented the efficacy of LDH-based materials for adsorptive removal of dyes from wastewater. Charafi *et al.*, successfully synthesized NiAl-LDH with Ni/Al molar ratio 2:1 and employed it in adsorptive removal of eriochrome black T dye.[16] The adsorption capacity of 37.71 mg/g was achieved with maximum adsorption in acidic environment. In another study, algae-modified ZnAl-LDH was prepared by Wibiyan *et al.*, for the mitigation of anionic dyes, with the optimal adsorption observed for methyl orange at 61.75% and 60.97% for congo red.[17] Mujtaba *et al.*, reported the fabrication of starch-impregnated MgAl-LDH (S/MgAl-LDH) for mitigation of methylene blue (MB) dye.[18] The adsorptive removal of MB achieved 73.15% for pristine MgAl-LDH and 89.71%

for S/MgAl-LDH within 120 min. Nevertheless, the adsorbent's performance for MB was limited by its efficacy being restricted to elevated pH values. Despite numerous reports on the application of LDHs as adsorbents in wastewater remediation, achieving ultrafast adsorption kinetics with consistently high efficiency across diverse pH environments remains a critical challenge.

Prior reports have reported successful incorporation of rare earth elements into LDH frameworks, which effectively increase the number of active sites and consequently result in improved adsorptive performance. In a work reported by Yuan *et al.,* La-Ca/Fe-LDH was fabricated by loading of La through impregnation.[19] The incorporation of La enhanced the adsorptive capacity of material by 11.4% than pristine Ca/Fe-LDH. In a separate investigation, Ce doped NiAl-LDH was synthesized by Wagassa *et al.,* using different amounts of Ce.[20] In another work, Barreto *et al.,* developed rare earth 3D hydroxide framework doped with Eu^{3+} ions and investigated the performance of the adsorbent for methyl orange, with maximum adsorption upto 70%.[21] Nevertheless, a significant research gap exists regarding the doping of rare earth elements to boost the adsorptive capacity in LDHs.

Based on existing literature, the fabrication of La doped NiAl-LDH for adsorptive removal of FG has not yet been investigated. In this work, the primary objective was to develop La/NiAl-LDH as a novel adsorbent with structural stability, capable of exhibiting superior performance across a wide pH range to eradicate FG from aqueous environment. Recyclability studies were conducted to determine the long-term suitability of La/NiAl-LDH for removal of FG from aqueous media.

2. Materials and Methods

2.1. Materials

Nickel nitrate hexahydrate ($Ni(NO_3)_2.6H_2O$), aluminium nitrate nonahydrate ($Al(NO_3)_2.9H_2O$) were purchased from CDH Pvt. Ltd. Lanthanum nitrate hexahydrate ($La(NO_3)_3.6H_2O$), sodium bicarbonate ($NaHCO_3$) and sodium hydroxide (NaOH, 97.0%) were purchased from Thermofisher Scientific. Fast green ($C_{37}H_{34}N_2Na_2O_{10}S_3$) was procured from Dyestar Pvt. Ltd.

2.2. Preparation of La/NiAl-LDH

The La-doped NiAl-LDH was synthesized via co-precipitation method. Solution containing 2 M NaOH and 1 M $NaHCO_3$ was slowly added to the aqueous solution of $Ni(NO_3)_2.6H_2O$ (0.75 M), $Al(NO_3)_3.9H_2O$ (0.24375 M) and $La(NO_3)_3.6H_2O$ (0.00625 M), until the pH

reached 10. The resulting suspension was aged in open atmosphere at 80 ˚C for 3 h with 400 rpm stirring rate, centrifuged and thoroughly rinsed with distilled water and ethanol. Subsequently, the final material was vacuum dried at 65 ˚C for 15 h and labelled as La/NiAl-LDH.

2.3. Adsorption assay of La/NiAl-LDH

To evaluate the efficacy of La/NiAl-LDH as adsorbent, FG was selected as the typical food dye contaminant. The absorption of FG was quantified using UV-visible spectrophotometer at absorption maxima wavelength of 625 nm. The extent of pollutant removal was determined using Eq. (1):[10]

$$\%A = \frac{(C_o - C_t)}{C_o} \times 100 \quad [1]$$

where *%A*, C_o (mg/L) and C_t stands for the percentage of dye adsorbed, initial concentration and concentration of dye at time, *t* respectively.

2.4. Adsorption studies

The fabricated La/NiAl-LDH was explored for the adsorptive uptake of FG from wastewater. The experiments were conducted with 100 mL of FG solution under optimal conditions at constant stirring for 10 min to ensure equilibrium. At fixed time intervals, 3mL aliquots of the solution were withdrawn to examine progressive adsorption advancement of FG. The sample collected was immediately centrifuged and supernatant was then analysed using UV-vis spectrophotometer. All the experiments were replicated atleast three times to ensure the reproducibility of the outcomes.

2.5. Characterization

The as-prepared sample was characterized by employing various techniques to ensure the successful synthesis. Powder X-ray diffractogram (P-XRD) was attained using PANalytical's X′Pert Pro diffractometer, Scan angle range: 5-80˚. The presence of various functional groups in synthesized material was analysed employing Fourier transform Infrared (FT-IR) spectrophotometer (PerkinElmer, scan range: 4000-400 cm^{-1}). Field emission scanning electron microscopy (FE-SEM) and energy dispersive X-ray spectrum (EDS) were collected to examine the surface morphology and elemental distribution of the material using Hitachi-SU8010 instrument. BET data was recorded by using Autosorb IQ-XR BET analyser. Thermogravimetric analysis (TGA) was performed through a Setaram instrument (model: Setsys). Adsorption reactions were monitored using JASCO (Model V-750) UV-visible spectrophotometer.

3. Results and Discussion

3.1. Characterization studies

3.1.1. Powder X-ray diffraction (P-XRD) analysis

The crystal structure of fabricated nanomaterial was assessed via P-XRD and the XRD pattern of La/NiAl-LDH is given in Fig. 1. The typical hydrotalcite-like pattern was observed with pronounced crystallinity. The strong characteristic peaks observed at 2θ = 11.6˚, 23.4˚, 34.9˚, 39.1˚, 46.4˚, 60.9˚ and 61.8˚, respectively assigned to the planes (003), (006), (012), (015), (018), (110) and (113) matched well with the reported literatures.[22, 23] Furthermore, the absence of any additional diffraction peak established phase purity of the material.

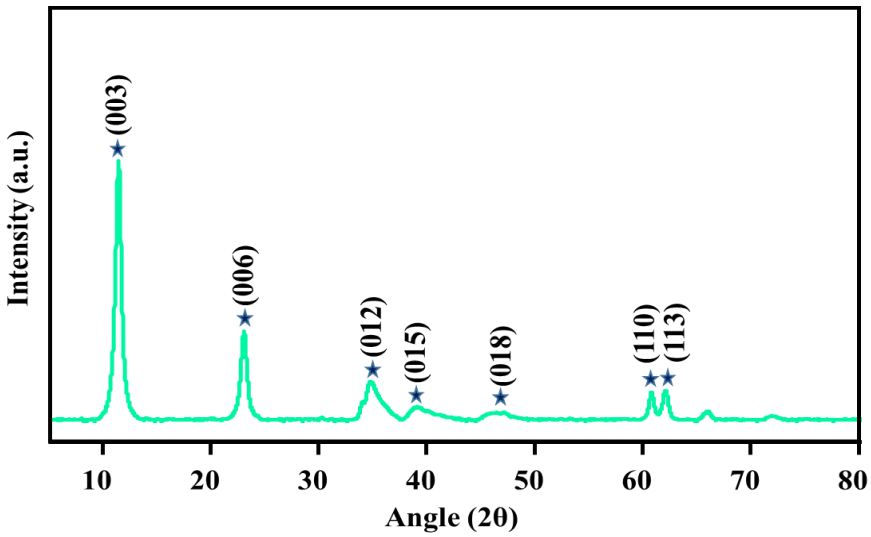

Fig. 1. P-XRD pattern of La/NiAl-LDH.

3.1.2. Fourier transform infrared spectroscopy (FT-IR)

To scrutinize the surface functionalities in La/NiAl-LDH, FT-IR was performed. As portrayed in Fig. 2., the broad band noted at 3462 cm^{-1} was ascribed to O-H stretching vibrations due to structural hydroxyl groups and interlayer water molecules; while a less intense band at 1627 cm^{-1} was assigned to bending vibrations of O-H bond of water molecules.[24] The stretching band detected at 1360 cm^{-1} signified the absorption peak of CO_3^{2-} intercalated in LDHs.[25] In addition, the bands located below 800 cm^{-1} could be ascribed to M-O-M or M-OH vibrations.[22, 24] Eventually, the successful engineering of La/NiAl-LDH via co-precipitation was evidenced by the characteristic bands of LDH in the FT-IR spectrum, uniform with the P-XRD data.

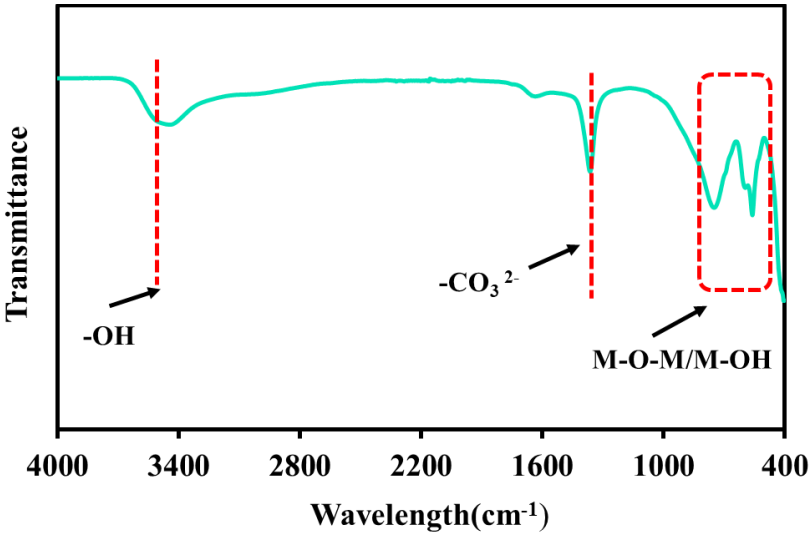

Fig. 2. FT-IR spectrum of La/NiAl-LDH.

3.1.3. Field emission Scanning Electron Microscopy (FE-SEM)

The morphology of La/NiAl-LDH was investigated using FE-SEM analysis and micrographs with high and low magnification are shown in Fig. 3(a & b), respectively.

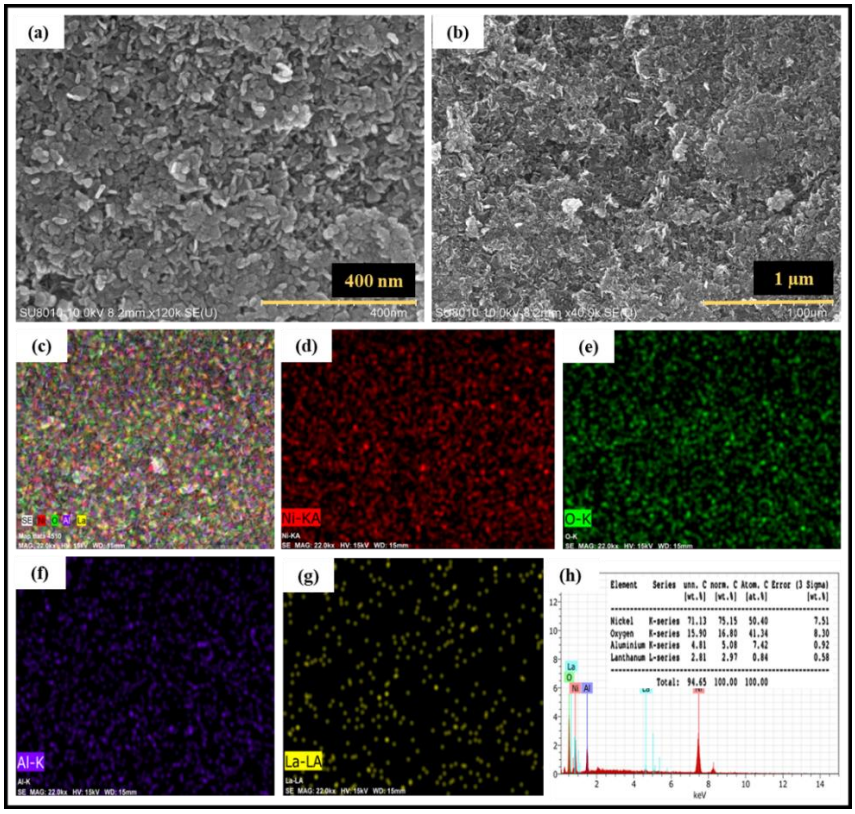

Fig. 3. (a, b) FE-SEM micrographs; (c) elemental mapping of La/NiAl-LDH, (d) Ni distribution, (e) O distribution, (f) Al distribution, (g) La distribution; (h) EDS spectra of La/NiAl-LDH.

The high magnification FE-SEM image of La/NiAl-LDH clearly showcased the presence of randomly oriented nano-ranged particles stacked in the form of thin sheets. The abundant intercalated anions provided substantial surface area and a microporous network, creating a perfect lamellar framework. To assess compositional uniformity, elemental mapping was performed and as demonstrated in Fig. 3(c-g), the target elements were homogenously dispersed throughout the material. Further, EDS analysis was employed to investigate the elemental composition of La/NiAl-LDH. The EDS spectrum (Fig. 3(h)) showcases the presence of only the intended elements, suggesting its high purity.

3.1.4. Thermogravimetric analysis (TGA)

The thermal stability and degradation profile of La/NiAl-LDH was examined by TGA in the range of 25-800 ˚C and the thermogram of the fabricated material is given in Fig. 4. The thermogram identified three major distinguishable mass loss stages in thermal decomposition of La/NiAl-LDH.[22] At first stage, mass loss of around 15% at temperature below 250 ˚C was possibly due to desorption of intercalated as well as the adsorbed water molecules. The mass loss of around 34% at second stage (from 275 ˚C) was assigned to dehydration of metal hydroxides and calcination of carbonates. At last stage, the formation of metal oxides due to collapse of La/NiAl-LDH structure was observed after 400 ˚C.[26]

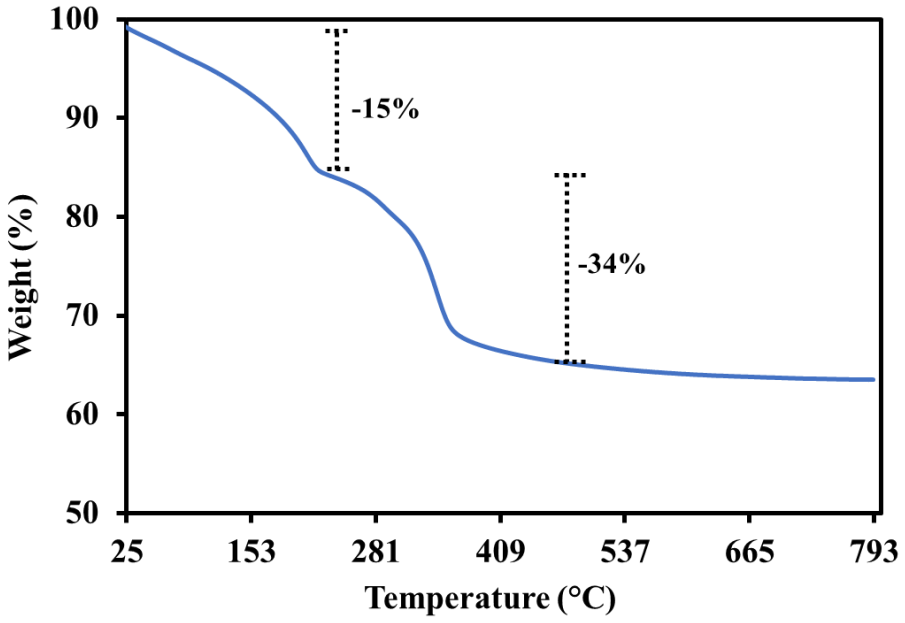

Fig. 4. TGA thermogram of La/NiAl-LDH nanomaterial.

3.1.5. Brunauer-Emmett-Teller (BET) analysis

The surface area is a critical property in evaluating the efficacy of adsorbent nanomaterials. To quantify this parameter, BET method was employed for La/NiAl-LDH adsorbent where the sample was degassed before analysis, using N_2 for 5 h at 100 ˚C. Fig. 5(a) presented the N_2 adsorption-desorption isotherm and BJH pore size distribution curve (inset) of the nanomaterial. The isotherm could be classified as a type IV adsorption isotherm with H3 hysterisis loop, depicting monolayer adsorption at low pressure and multilayer adsorption at high pressure for the adsorbent.[2, 27] Furthermore, the BJH curve in Fig. 5(a) (inset) suggests a predominance of mesopores, leading to an adequate adsorption capacity. The BET results revealed the total surface area of La/NiAl-LDH was 86.1 m^2/g with pore diameter and pore volume of 2.9 nm and 0.198 cm^3/g, respectively. In addition, validity of the calculated surface area of La/NiAl-LDH was confirmed by the strong linearity of corresponding BET plot across the established relative pressure range (Fig 5(b)).

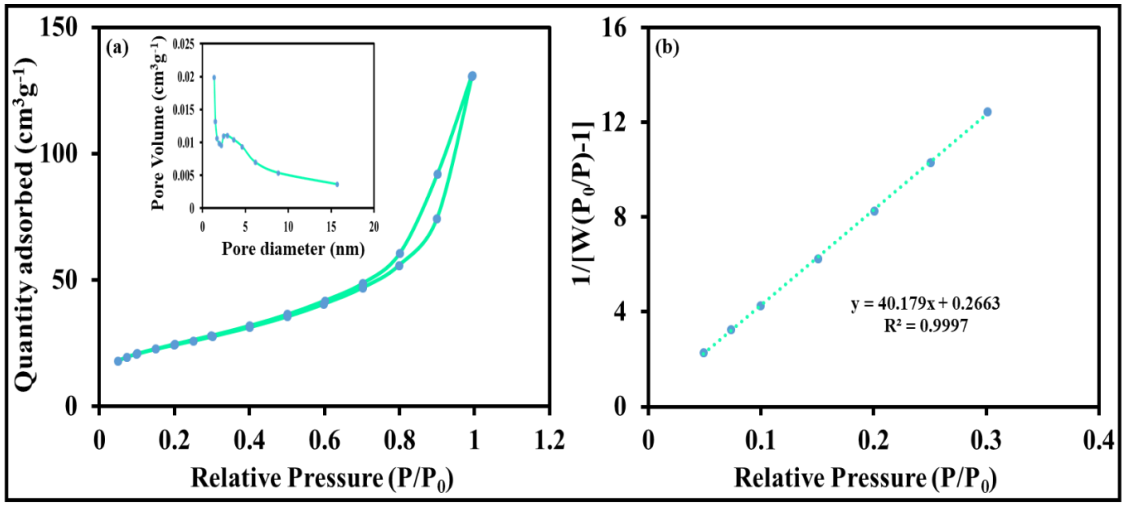

Fig. 5. (a) N_2 adsorption-desorption plot and BJH curve (inset), (b) BET plot of La/NiAl-LDH.

3.2. Adsorption screening

3.2.1. Influence of reaction parameters

3.2.1.1. Effect of contact time

The effect of contact time on performance of La/NiAl-LDH for removal of FG was examined with fixed adsorbent amount of 25 mg in FG solution (100 mL, initial concentration of 10 mg/L at neutral pH). The result demonstrated in Fig. 6(a) depicted that the maximum adsorptive uptake of around 80% for FG was within 2 min, evidencing the ultrafast adsorptive performance of La/NiAl-LDH. After some time, there was a gradual

increase in adsorption percentage with the maximum removal of 94% achieved in 10 min. Hereafter, an optimum contact time of 10 min was selected for further investigations. Under identical conditions, reaction was performed with pristine NiAl-LDH and the maximum adsorption percentage achieved at equilibrium was 78% only.

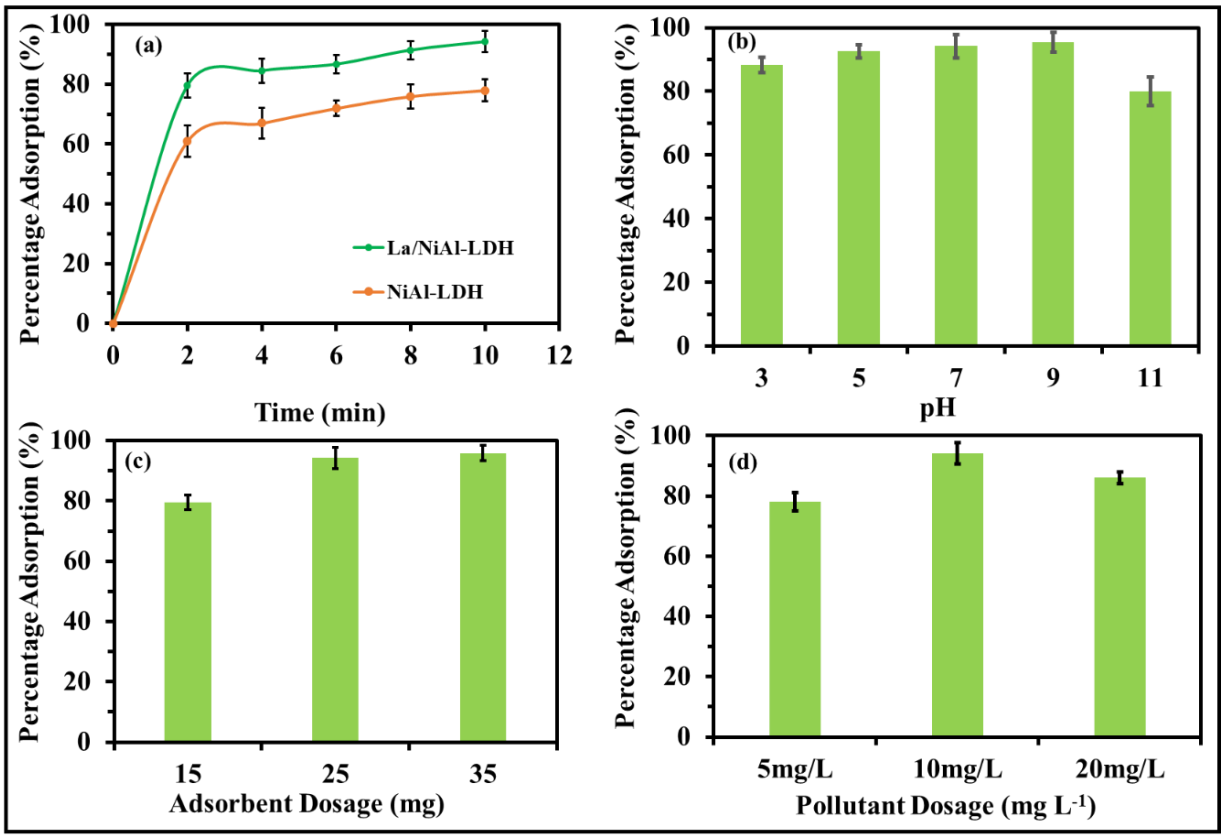

Fig. 6. (a) Effect of contact time, (b) pH, (c) catalyst dosage and adsorbate concentration on adsorption percentage of FG.

3.2.1.2. Effect of pH

The impact of pH of solution on the adsorptive performance of La/NiAl-LDH was examined in the pH range of 3-11 and the outcomes have been demonstrated in Fig. 6(b). It is evident that the adsorbent exhibited excellent performance across entire pH range, highlighting its superior adsorption capacity. The zeta potential studies (Fig. 7.) revealed the presence of positive charge in range of 5-9, showcasing strong electrostatic interactions with negatively charged FG molecules. La/NiAl-LDH exhibited maximum adsorptive uptake at pH 9; however, its efficacy at neutral pH was comparable. Consequently, the remaining studies were carried out at neutral pH.

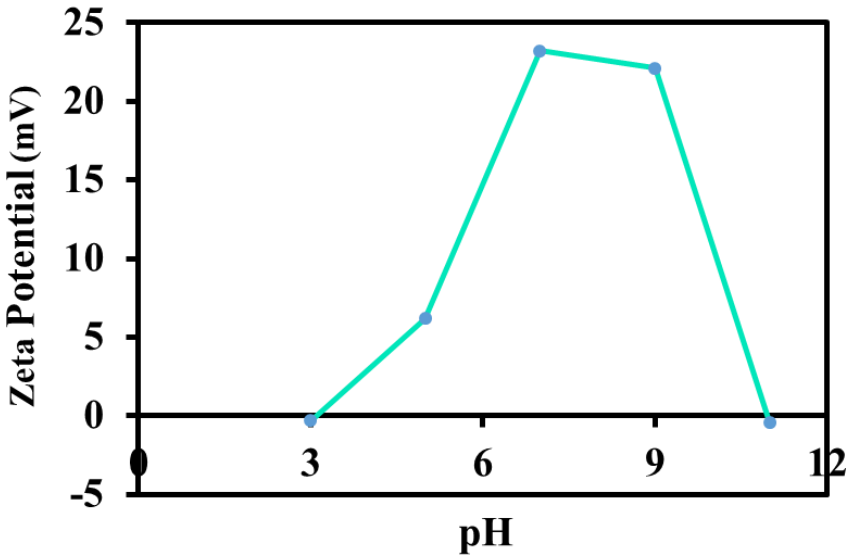

Fig. 7. Zeta potential of La/NiAl-LDH at pH = 3, 5, 7, 9 and 11.

3.2.1.3. Effect of catalyst dosage

Adsorbent dosage directly relates to the number of free adsorption sites and availability of surface area. To achieve maximum adsorption results, effect of adsorbent dosage was investigated. Fig. 6(c) depicts that as the adsorbent dosage augmented from 15 mg to 25 mg, there was a significant escalation in the adsorption percentage from approximately 79% to 94%. However, when the adsorbent dosage was increased from 25 mg (94%) to 35 mg (96%), no significant escalation was observed. During early phase of adsorption, many adsorption sites remain unoccupied and readily available; hence, more pollutant removal can be observed. With continued increase in adsorbent dosage, particle clustering becomes prominent, resulting in no significant improvement. Therefore, 25 mg of La/NiAl-LDH was chosen as optimum quantity for further studies.

3.2.1.4. Effect of adsorbate concentration

The effect of initial adsorbate concentration was examined and the results are given in Fig. 6(d). Keeping the other conditions predetermined, the initial concentration of FG was varied from 5 to 20 mg/L. Apparently, the removal percentage increased markedly as the adsorbate concentration was raised from 5 mg/L (78%) to 10 mg/L (94%), owing to the availability of large number of active sites. However, a decrease in removal percentage (86%) was observed when pollutant concentration was further increased to 20 mg/L, which resulted due to saturation of adsorbent sites and intensified competition among FG molecules.[28]

3.2.1.5. Simulated real sample analysis

To validate the effectiveness of La/NiAl-LDH beyond ideal laboratory conditions, the adsorption studies were conducted using real water matrices. The real water samples were collected from different water sources, which include tap water from lab, river water from the Ganga (Haridwar) and lake water from Sukhna Lake (Chandigarh).[10] The collected samples were filtered to remove any suspended impurities and spiked with FG pollutant. The results, as depicted in Fig. 8., demonstrated consistently high adsorption proficiency of La/NiAl-LDH in all type of real water samples. These findings suggest that the adsorption performance remained largely unaffected by different water samples, rendering La/NiAl-LDH as a suitable adsorbent in removing FG even in complex environments.

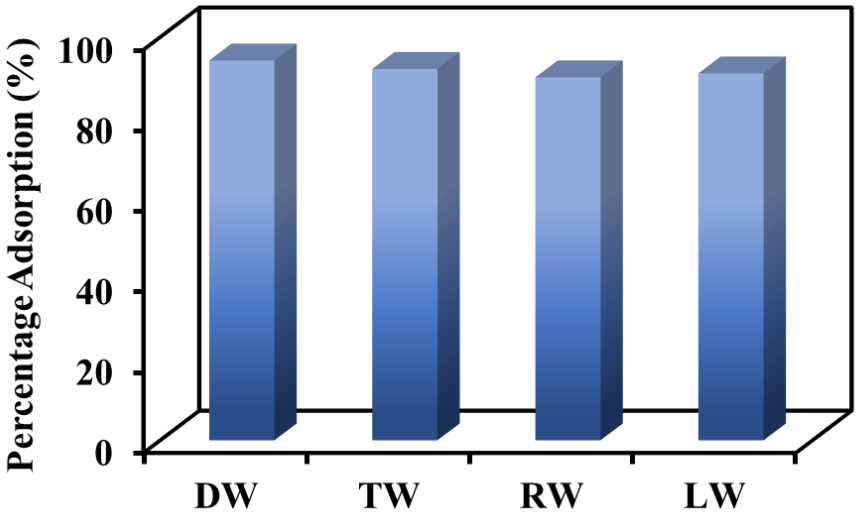

Fig. 8. Influence of real water samples on removal percentage of FG using La/NiAl-LDH.

3.2.2. Adsorption isotherm studies

To understand the interactions of FG with La/NiAl-LDH and to elucidate adsorption mechanism, Langmuir and Freundlich models were used to fit the experimental data. The linear and non-linear form of Langmuir and Freundlich isotherm model is represented by Eq. (2-5), respectively:

Langmuir model:

$$\frac{C_e}{q_e} = \frac{1}{K_L q_{max}} + \frac{C_e}{q_{max}} \quad [2]$$

$$q_e = \frac{q_{max} K_L C_e}{1 + K_L C_e} \quad [3]$$

Freundlich model:

$$logq_e = logK_F + \frac{1}{n} logC_e \quad [4]$$

$$q_e = K_F C_e^{\frac{1}{n}} \quad [5]$$

where C_e (mg/L) refers to the concentration of dye at equilibrium; q_e (mg/g) is the adsorption capacity at equilibrium; q_{max} (mg/g) is the maximum adsorption capacity; K_L (L/mg) is the Langmuir constant; K_F ((mg/g) (L/mg)$^{1/n}$) is the Freundlich constant and n is the constant indicating intensity of adsorption. The dimensionless separation factor (R_L), is calculated to determine the favorability of adsorption process and the equation is given in Eq. (6):

$$R_L = \frac{1}{1+K_L C_0} \quad [6]$$

The adsorption phenomenon is considered unfavourable if R_L>1, R_L=1 suggests linearity; 0<R_L<1 specifies favorability and R_L= 0 signifies irreversibility.[10,28] As depicted from Fig. 9(a, b) and tabulated data in Table 1., the R^2 value of La/NiAl-LDH depicted an excellent fit with the Langmuir adsorption isotherm compared to the Freundlich isotherm, suggesting monolayer adsorption. The isotherm models with non-linear fittings (Fig. 11(a)) also supported the dominance of Langmuir adsorption isotherm over Freundlich isotherm model. The maximum adsorption capacity (q_{max}) obtained for FG from Langmuir plot was 17.88 mg/g.

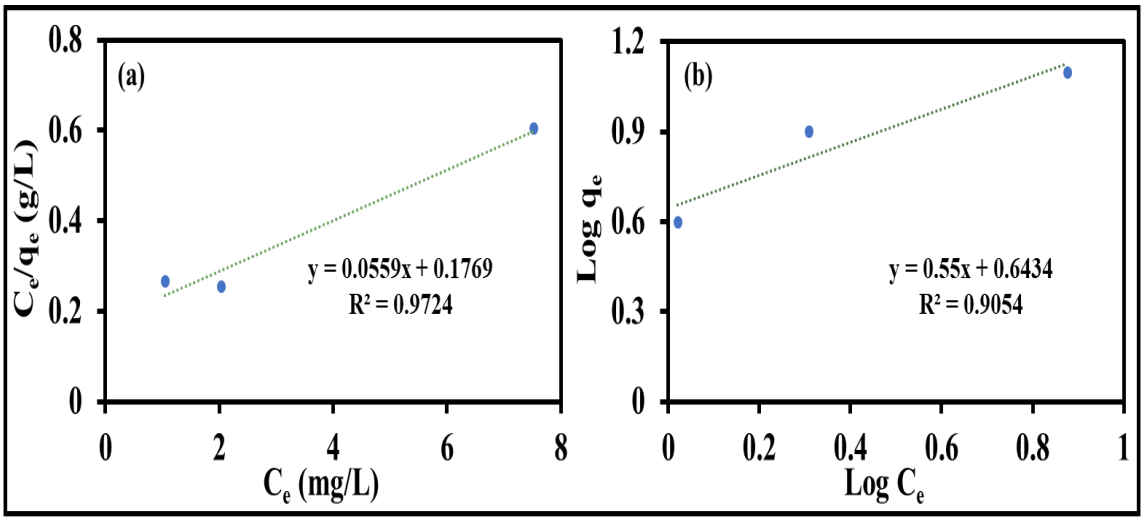

Fig. 9. Plot of linear (a) Langmuir; (b) Freundlich adsorption isotherm.

Table 1. Adsorption isotherm data for adsorption of FG on surface of La/NiAl-LDH in linear and non-linear form.

Model	Parameters	Pollutant (FG)	
		Linear form	Non-Linear form
Langmuir	R^2	0.972	0.970
	K_L (L/mg)	0.315	0.353 ± 0.141
	R_L	0.240	0.221 ± 0.069
	q_{max} (mg/g)	17.889	17.350 ± 2.923
Freundlich	R^2	0.905	0.933
	K_F ((mg/g) (L/mg)$^{1/n}$)	4.399	4.872 ± 1.161
	N	1.818	2.110 ± 0.625

3.2.3. Adsorption kinetic studies

In this work, the pseudo first order and pseudo second order kinetic models were applied to fit experimental data. The mathematical linear and non-linear equations representing pseudo first order and pseudo second order kinetic models are given in Eq. (7-10), respectively:

Pseudo first order kinetic model in linear and non-linear form:

$$log(q_e - q_t) = log q_e - \frac{K_1 t}{2.303} \quad [7]$$

$$q_t = q_e(1 - \exp(K_1 t)) \quad [8]$$

Pseudo second order kinetic model in linear and non-linear form:

$$\frac{t}{q_t} = \frac{1}{K_2 q_e^2} + \frac{t}{q_e} \quad [9]$$

$$q_t = \frac{q_e K_2 t}{q_e K_2 t + 1} \quad [10]$$

where q_t is the adsorption capacity at contact time t (min); K_1 (min^{-1}) and K_2 (g/(mg min)) are the equilibrium rate constant for pseudo first order and pseudo second order kinetic model, respectively.[10] The related plots for both kinetic models in linear form and non-linear form have been stipulated in Fig. 10(a, b) and Fig. 11(b), respectively, where the adsorption kinetic parameters have been listed in Table 2.

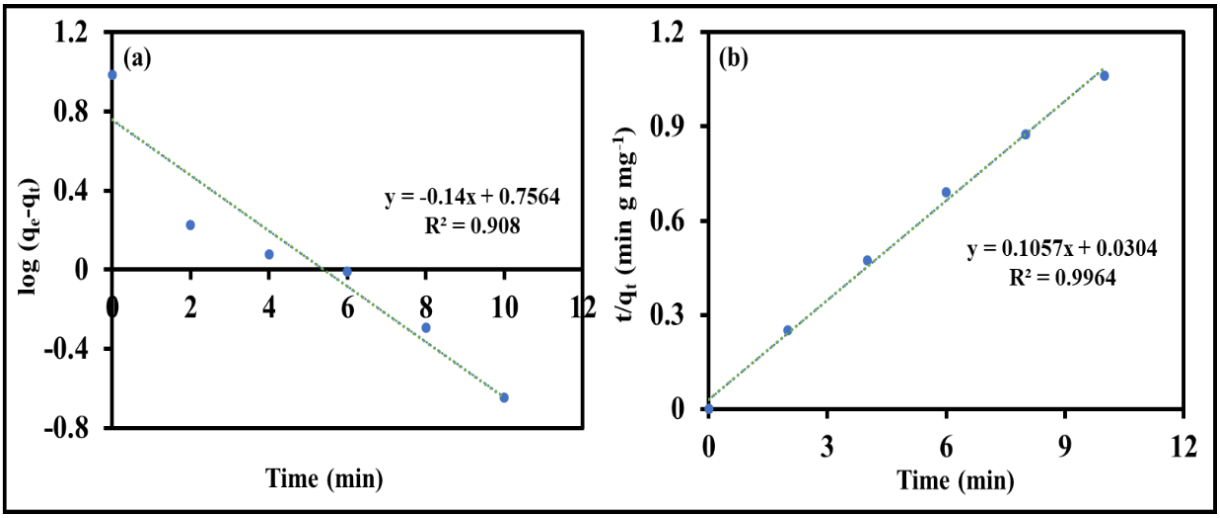

Fig. 10. Linear (a) pseudo first order and (b) pseudo second order kinetics plot.

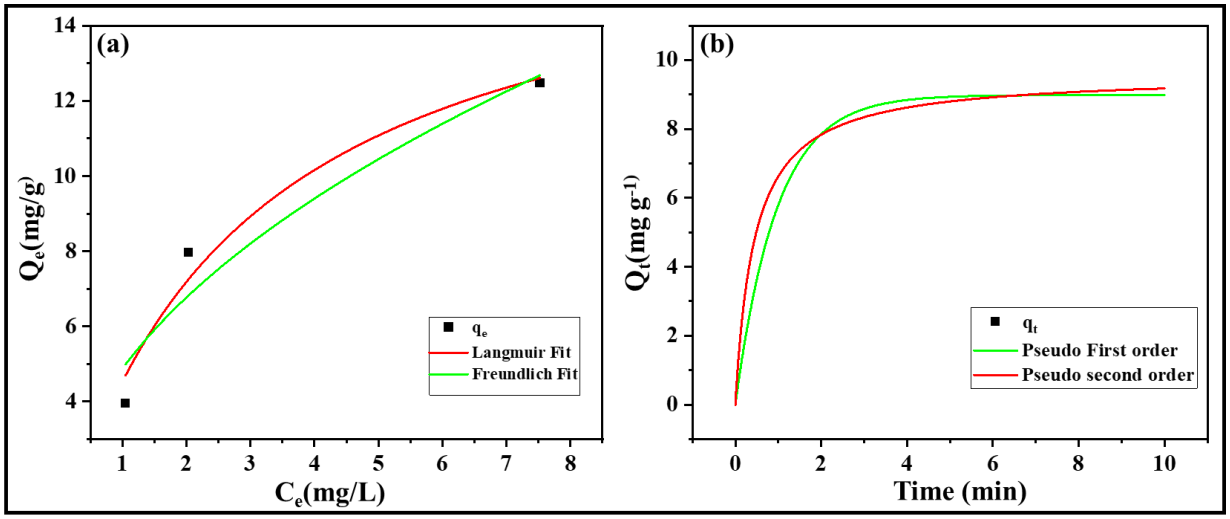

Fig. 11. Non-linear (a) Langmuir & Freundlich isotherm; (b) pseudo first order & pseudo second order kinetics plot.

The plot clearly demonstrated a better fitting curve for pseudo second order kinetics model (R^2 = 0.996) than for pseudo first order kinetics model (R^2 = 0.908) in both linear and non-linear fittings. Thus, it revealed that the adsorption process may involve chemisorption. A comparative study with other reported FG adsorbents along with this work is tabulated in Table 3.

Table 2. Various reaction kinetics parameters in linear and non-linear form.

Model	Parameters	Pollutant (FG)	
		Linear form	Non-Linear form
Pseudo first order	R^2	0.908	0.990
	K_1 (min^{-1})	0.322	1.034 ± 0.171
	q_e (mg/g)	5.706	8.986 ± 0.185
Pseudo second order	R^2	0.992	0.997
	K_2 (g/(mg min))	0.367	0.233 ± 0.056
	q_e (mg/g)	9.460	9.588 ± 0.208

Table 3. A comprehensive table comparing various FG adsorbents.

FG Adsorbent	Maximum adsorption capacity(mg/g)	Time(min)	Adsorption Percentage (%)	Reference
$NiCo_2O_4$@g-C_3N_4	3.72 mg/g	60 min	95.38%	[29]
Fe_3O_4 MNPs	7.4 mg/g	75 min	86.31%	[30]
M-biochar	0.78 mg/g	60 min	97%	[31]
MN-biochar	2.13 mg/g	60 min	97%	[31]
MZ-biochar	12.44 mg/g	60 min	99%	[31]
La/NiAl-LDH	17.9 mg/g	10 min	94%	**This Work**

3.2.4. Mechanism

A probable mechanism for adsorption of FG on the surface of La/NiAl-LDH can be elucidated using insights obtained from adsorption isotherms, kinetic data, zeta potential and FT-IR spectra. The FT-IR analysis was performed before and after adsorption and the spectra has been demonstrated in Fig. 12. The Langmuir adsorption isotherm revealed that the adsorption was monolayer and homogeneous in nature. Moreover, the pseudo second order kinetics model depicted possibility of chemisorption contribution. Additionally, the zeta potential studies showcased highly positive surface charge of the adsorbent in pH range

of 5-9, favouring strong electrostatic interaction with anionic FG molecules. Evidently, the presence of numerous pores as depicted by FE-SEM and BET results, offered readily available active sites for adsorbate molecules. Further, decrease in intensity of –OH groups present on La/NiAl-LDH after adsorption as evidenced from FT-IR data, suggested the involvement of hydrogen bonding interactions.

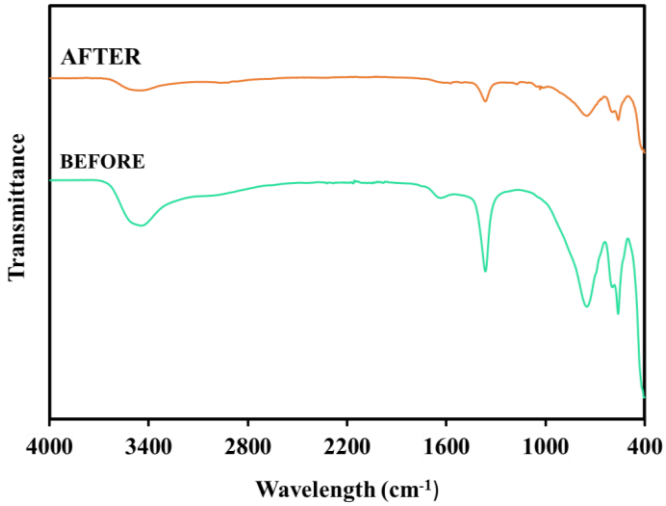

Fig. 12. FT-IR spectra of La/NaAl-LDH before and after adsorption of FG.

3.3. Regeneration and reusability studies

To determine the long-term suitability of La/NiAl-LDH for various wastewater treatment applications, regeneration studies were performed. The desorption experiments were performed for removing FG from surface of La/NiAl-LDH in a (1:1) mixture of HCl and NaCl solution. For desorption, 5 mg of dye loaded adsorbent was shaken in 30 mL of desorbing solution for 30 min. After that, the collected sample was kept on drying at 60 ˚C for 5 h for use in other experiments. The reusability of La/NiAl-LDH was tested four times as shown in Fig. 13. The extraordinary retention in adsorption capacity of La/NiAl-LDH for FG even after 4 cycles (above 75%) showcases it as a potential material for sequestration of toxic pollutants from aqueous media.

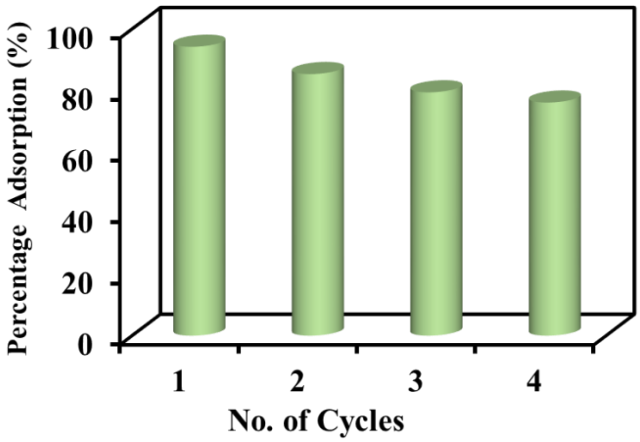

Fig. 13. Recyclability plot for the adsorption of FG over La/NiAl-LDH nanomaterial.

The P-XRD analysis was performed for regenerated adsorbent (Fig. 14.), where the characteristic peaks of material were retained suggesting stable structural properties of the material.

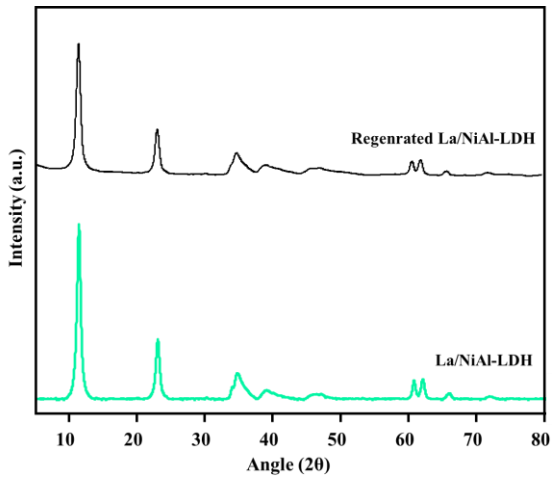

Fig. 14. P-XRD of La/NiAl-LDH before adsorption and regenerated La/NiAl-LDH.

4. Conclusions

La doped NiAl-LDH (La/NiAl-LDH) was fabricated for the mitigation of FG from wastewater. The synthesized material was characterized by employing various techniques such as FE-SEM, P-XRD, FT-IR, BET and TGA. The material exhibited high surface area, porosity, thermal stability and exceptional regenerability. The synthesized nanomaterial was tested for its ability to adsorb FG, where the ultrafast adsorption of 94% was achieved within 10 min. The adsorption isotherm and kinetics studies demonstrated that the Langmuir isotherm and pseudo second order model fits well with the adsorption process. Overall, utilizing La/NiAl-LDH as an adsorbent offers a promising approach for concomitant adsorption of FG from aqueous media.

Acknowledgements

The authors are extremely thankful to the University Grant Commission (UGC), India (R. No.: HR0602510322, Ref. No.: 221610005994), Department of Science and Technology (DST), India (Sanction No. WTC/OWUIS-2021/RS-09(G)), for financially supporting the research work. The authors would like to thankfully acknowledge the Sophisticated Analytical Instrumentation Facility (SAIF-CIL), Panjab University, Chandigarh, for the required instrumental facilities.

Authors' contributions

Minakshi: Conceptualization, Visualization, Data curation, Formal analysis and Writing the original draft; Aarti: review & editing; Sonal Singhal: Supervision, Validation, Resources, review & editing.

Conflict of interest

The authors affirm that they have no known financial conflicts or personal affiliations that could have influenced the work presented in this paper.

References

1. T. Garg, Movikiran, Nitansh, S. Kaur, B. Singh, S. Singhal, 'Unlocking the photo-Fenton potential of novel magnetically separable sulfur doped g-C_3N_4/$CoFe_2O_4$ Z-scheme heterojunction systems towards tetracycline removal', J. Sol-Gel Sci. Technol., 112, 94-111, 2024.
2. Nidhi, D. Sharma, Minakshi, S. Kaur, S. Bansal, P. Kaur, S. Singhal, 'Building a potentially active $NiFe_2O_4$ embedded lignin framework for adsorption coupled photocatalytic degradation and fluorescence detection of doxorubicin and safranin-O', React. Funct. Polym., 219, 106589-106603, 2025.
3. Y.X. Chen, Y.M. Yuan, H.Y. Yang, Q. Wang, Y. Ren, X.H. Guo, P. Zhang, M.J. Zhang, W. Wang, L.Y. Chu, 'Hierarchical porous tannic-acid-modified MOFs/alginate particles with synergized adsorption-photocatalysis for water remediation', Sep. Purif. Technol., 330, 125435-125449, 2024.
4. Sachin, B.K. Pramanik, H. Gupta, S. Kumar, J.S. Tawale, K., Shah, E. Varathan, N. Singh, 'Development of a ZnOS+C composite as a potential adsorbent for the effective removal of fast green dye from real wastewater', ACS omega, 8, 9230-9238, 2023.
5. Nidhi, Ekta, P. Kaur, K. Thakur, A. Sheoran, S. Singhal, 'Probing the photo-Fenton potential of magnetically recoverable lignin incorporated nickel ferrite

nanocomposites for mitigation of synthetic textile dye', Res. Chem. Intermed., 51, 7161-7183, 2025.

6. X. Wang, J. Li, L. Xu, J. Su, Z. Wang, X. Li, 'Simultaneous removal of calcium, cadmium and tetracycline from reverse osmosis wastewater by sycamore deciduous biochar, shell powder and polyurethane sponge combined with biofilm reactor', Bioresour. Technol., 394, 130215-130225, 2024.
7. D. Yanardağ, S. Edebali, 'Adsorptive removal of malachite green dye from aqueous solution by ion exchange resins', BioConvers Biorefin, 14, 5699-5710, 2024.
8. A.S. Abdulhameed, R.H. Al Omari, S. Althahban, Y. Jazaa, M. Abualhaija, S. Algburi, 'Green vegetable waste composited with chitosan as a bioadsorbent for effective removal of methylene blue dye from water: Insight into physicochemical and adsorption characteristics', Biomass and Bioenergy, 193, 107528-107540, 2025.
9. S. Kaur, T. Garg, Abhivyakti, Sonam, Nitansh, S. Rana, S. Singhal, N. Goel, 'Engineering Multifunctional S-Scheme Sn-MOF/$NiFe_2O_4$ Heterostructure for Abolition and Detection of Contaminants: In-Silico Ecotoxicity Assessment and DFT-Assisted Mechanism Elucidation', Adv. Sustain. Syst., 9, 00610-00628, 2025.
10. Minakshi, D. Aggarwal, Abhivyakti, Nidhi, P. Kaur, S. Singhal, 'Floral waste-derived biochar functionalized with SDS: A bifunctional material for integrated adsorptive removal and fluorescent detection of deleterious pollutants', Process Saf. Environ. Prot., 204, 108037-108053, 2025.
11. T. Shahryari, P. Singh, P. Raizada, A. Davidyants, L. Thangavelu, S. Sivamani, A. Naseri, F. Vahidipour, A. Ivanets, A. Hosseini-Bandegharaei, 'Adsorption properties of Danthron-impregnated carbon nanotubes and their usage for solid phase extraction of heavy metal ions', Colloids Surf., 641, 128528-128537, 2022.
12. T. Rasheed, F. Kausar, K. Rizwan, M. Adeel, F. Sher, N. Alwadai, F.H. Alshammari, 'Two dimensional MXenes as emerging paradigm for adsorptive removal of toxic metallic pollutants from wastewater', Chemosphere, 287, 132319-132328, 2022.
13. C. Xia, H. Huang, D. Liang, Y. Xie, F. Kong, Q. Yang, J. Fu, Z. Dou, Q. Zhang, Z. Meng, 'Adsorption of tetracycline hydrochloride on layered double hydroxide loaded carbon nanotubes and site energy distribution analysis', Chem. Eng. J., 443, 136398-136407, 2022.

14. D. Li, M. Chen, Y. Jiang, 'Adsorptive removal of phosphate by ZnAlLa ternary layered double hydroxides: Synthesis conditions, adsorption performance, mechanism and reusability', Sep Purif Technol, 354, 128668-128680, 2025.
15. A.M. Ramezani, F.A. Panah, M.H. Dokoohaki, E.A. Azooz, R. Ahmadi, S. Nazari, 'Zn/Ce-layered double hydroxide for adsorptive removal of doxycycline from water', Mater. Chem. Phys., 318, 129223-129234, 2024.
16. S. Charafi, F.Z. Janani, A. Elhalil, M. Abdennouri, M. Sadiq, N. Barka, 'Adsorption and reusability performances of Ni/Al layered double hydroxide for the removal of Eriochrome Black T dye', Biointerface Res. Appl. Chem, 13, 265-271, 2023.
17. S. Wibiyan, I. Royani, N. Ahmad, A. Lesbani, 'Assessing the efficiency, selectivity, and reusability of ZnAl-layered double hydroxide and Eucheuma cottonii composite in removing anionic dyes from wastewater', Inorg. Chem. Commun., 170, 113347-113359, 2024.
18. G. Mujtaba, A. Ullah, D. Khattak, M.U.H. Shah, M. Daud, S. Ahmad, A. Hai, F. Ahmed, T. Alshahrani, F. Banat, 'Simultaneous adsorption of methylene blue and amoxicillin by starch-impregnated MgAl layered double hydroxide: Parametric optimization, isothermal studies and thermo-kinetic analysis', Environ. Res., 235, 116610-116621, 2023.
19. M. Yuan, S. Qiu, M. Li, Z. Di, M. Feng, C. Guo, W. Fu, K. Zhang, W. Hu, F. Wang, 'Enhancing phosphate removal performance in water using La–Ca/Fe–LDH: La loading alleviates ineffective stacking of laminates and increases the number of active adsorption sites', J. Clean. Prod., 388, 135857-135866, 2023.
20. A.N. Wagassa, T.A. Shifa, A. Bansiwal, E.A. Zereffa, 'Kinetics, isotherm, mechanism, and recyclability of novel nano-sized Ce^{4+}-doped Ni–Al layered double hydroxide for defluoridation of aqueous solutions', Environ. Sci. Pollut. Res. Int, 30, 119084-119094, 2023.
21. A.S. Barreto, K.O. Moura, M.D.C.S. Barreto, S.A. Júnior, 'Luminescence of rare earth 3D hydroxide framework Eu^{3+}-doped and its application in dye adsorption tests', Appl. Clay Sci., 245, 107128-107136, 2023.
22. H. Mkaddem, E. Rosales, M. Pazos, H.B. Amor, M.A. Sanromán, J. Meijide, 'Anti-inflammatory drug diclofenac removal by a synthesized MgAl layered double hydroxide', J. Mol. Liq., 359, 119207-119217, 2022.

23. M. Bansal, K. Jasuja, R.K. Das, ‘Photocatalytic degradation of reactive dyes over NiAl layered double hydroxide’, Catal. Commun., 187, 106879-106887, 2024.

24. T. Li, X. Du, J. Deng, K. Qi, J. Zhang, L. Gao, X. Yue, ‘Efficient degradation of Rhodamine B by magnetically recoverable Fe_3O_4-modified ternary CoFeCu-layered double hydroxides via activating peroxymonosulfate’, J. Environ. Sci., 108, 188-200, 2021.

25. R. Elmoubarki, W. Boumya, F.Z. Mahjoubi, A. Elhalil, M. Sadiq, N. Barka, ‘Ni-Fe-SDS and Ni-Fe-SO_4 layered double hydroxides: Preparation, characterization and application in dyes removal’, Mater. Today Proc., 37, 3871-3875, 2021.

26. J. Kameliya, A. Verma, P. Dutta, C. Arora, S. Vyas, R.S. Varma, ‘Layered double hydroxide materials: A review on their preparation, characterization, and applications’, Inorganics, 11, 121-142, 2023.

27. A. Goyal, D. Aggarwal, S. Kapoor, N. Goel, S. Singhal, J. Shukla, ‘A comprehensive experimental and theoretical study on BN nanosheets for the adsorption of pharmaceutical drugs’, New J. Chem., 44, 3985-3997, 2020.

28. D. Aggarwal, H. Kaur, P. Kaur, Abhivyakti, B. Singh, S. Singhal, ‘Leveraging the multifaceted utility of Psidium guajava derived activated carbon: A sustainable strategy for adsorptive detoxification and real-time detection of pollutants in wastewater’, J. Water Process Eng., 72, 107490-107504, 2025.

29. A.K. Singh, S. Agrahari, R.K. Gautam, I. Tiwari, ‘A highly efficient $NiCo_2O_4$ decorated g-C_3N_4 nanocomposite for screen-printed carbon electrode based electrochemical sensing and adsorptive removal of fast green dye’, Environ. Sci. Pollut. Res. Int., 31, 67339-67354, 2024.

30. R.F. Abbas, M.J.M. Hassan, A.M. Rheima, ‘Adsorption of fast green dye onto Fe_3O_4 MNPs and GO/Fe_3O_4 MNPs synthesized by photo-irradiation method: isotherms, thermodynamics, kinetics, and reuse studies’, Sustain. Chem. Environ., 6, 100104-100118, 2024.

31. H. Park, J., Kim, Y.G. Lee, K. Chon, ‘Enhanced adsorptive removal of dyes using mandarin peel biochars via chemical activation with NH_4Cl and $ZnCl_2$’, Water, 13, 1495-1508, 2021.